International Journal of Pharmaceutics 572 (2019) 118756

Contents lists available at ScienceDirect

International Journal of Pharmaceutics

journal homepage: www.elsevier.com/locate/ijpharm

Prilling of API/fatty acid suspensions: Processability and characterisation

E. De Coninck[a], V. Vanhoorne[a], A. Elmahdy[b], M. Boone[c], G. Van Assche[d], D. Markl[e,f], B.G. De Geest[a], T. De Beer[g], C. Vervaet[a,*]

[a] Laboratory of Pharmaceutical Technology, Ghent University, Ghent, Belgium
[b] Materials Science and Technology – DyMaLab Research Group, Department of Electromechanical Systems and Materials, Ghent University, Zwijnaarde, Belgium
[c] Centre for X-ray Tomography (UGCT), Department of Physics and Astronomy, Ghent University, Ghent, Belgium
[d] Physical Chemistry and Polymer Science, Vrije Universiteit Brussel, Brussels, Belgium
[e] Strathclyde Institute of Pharmacy and Biomedical Sciences, University of Strathclyde, Glasgow, United Kingdom
[f] EPSRC Centre for Innovative Manufacturing in Continuous Manufacturing and Crystallisation, University of Strathclyde, Glasgow, United Kingdom
[g] Laboratory of Pharmaceutical Process Analytical Technology, Ghent University, Ghent, Belgium

ARTICLE INFO

Keywords:
Prilling
Controlled release
Multiparticulate dosage forms
Fatty acids
Metformin hydrochloride
Paracetamol

ABSTRACT

Current study evaluated the processability and characteristics of prills made of an active pharmaceutical ingredient/fatty acid (API/FA) suspension instead of previously studied API/FA solutions to enlarge the application field of prilling. Metformin hydrochloride (MET) and paracetamol (PAR) were used as model APIs while both the effect of drug load (10–40%) and FA chain length (C14–C22) were evaluated. API/FA suspensions were processable on lab-scale prilling equipment without thermal degradation, nozzle obstruction or sedimentation in function of processing time. The collected prills were spherical (AR ≥ 0.898) with a smooth surface (sphericity ≥ 0.914) and a particle size of ± 2.3 mm and 2.4 mm for MET and PAR prills, respectively, independent of drug load and/or FA chain length. In vitro drug release evaluation revealed a faster drug release at higher drug load, higher API water solubility and shorter FA chain length. Solid state characterisation via XRD and Raman spectroscopy showed that API and FA crystallinity was maintained after thermal processing via prilling and during storage. Evaluation of the similarity factor indicated a stable drug release (f_2 > 50) from MET and PAR prills after 6 months storage at 25 °C or 40 °C.

1. Introduction

Due to their biocompatibility, low toxicity, low cost and pharmaceutical approved status, lipids (e.g. oils, waxes, triglycerides, partial glycerides, fatty alcohols and fatty acids (FAs)) have gained interest in the pharmaceutical industry as versatile excipients to mask taste, protect unstable active pharmaceutical ingredients (APIs), increase the bioavailability and sustain the dissolution rate (Pivette et al., 2012; Rosiaux et al., 2014; Jannin et al., 2008; Reitz and Kleinebudde, 2007; Becker et al., 2015; Aleksovski et al., 2016). Solid lipid-based drug formulations can be produced via solvent-free melting techniques, such as melt extrusion, melt coating and spray congealing, all relatively short, cost-effective and environmentally friendly production processes (Jannin et al., 2008; Becker et al., 2015; Aleksovski et al., 2016; Vervaeck et al., 2015). Via spray congealing spherical microspheres consisting of a drug imbedded in a lipid matrix can be produced (Passerini et al., 2010; Martins et al., 2013). A specific type of spray congealing, called prilling, yields larger spherical particles (diameter > 500 µm) resulting in a slower controlled release system and excellent flow properties for volumetric capsule filling (Rosiaux et al., 2014; Becker et al., 2015; Séquier et al., 2014; Vervaeck et al., 2013).

Although prilling is widely applied in the agricultural industry for the production of urea beads (Mehrez et al., 2014; Rahamnian and Homayoonfard, 2012; Rahmanian et al., 2013; Rahmanian et al., 2015), its applications in the pharmaceutical field are limited as stated by Aleksovski et al. (2016). Pivette et al. examined the controlled-release

Abbreviations: API, active pharmaceutical ingredient; BA, behenic acid; FA, fatty acid; fps, frames per second; MA, myristic acid; MET, metformin hydrochloride; MPT, metoprolol tartrate; NA, not applicable; PA, palmitic acid; PAR, paracetamol; RH, relative humidity; RHC, rapid heat-cool differential scanning calorimetry; SA, stearic acid; SD, standard deviation; SEM, scanning electron microscopy; SLS, sodium lauryl sulfate; SNV, standard normal variate; TGA, thermogravimetric analysis; USP, United States Pharmacopeia; XRD, X-ray diffraction

* Corresponding author at: Laboratory of Pharmaceutical Technology, Ghent University, Ottergemsesteenweg 460, 9000 Ghent, Belgium. Tel.: +32 9 264 80 69.
E-mail addresses: elien.deconinck@ugent.be (E. De Coninck), valerie.vanhoorne@ugent.be (V. Vanhoorne), ahmed.elmahdy@ugent.be (A. Elmahdy), matthieu.boone@ugent.be (M. Boone), guy.van.assche@vub.be (G. Van Assche), daniel.markl@strath.ac.uk (D. Markl), br.degeest@ugent.be (B.G. De Geest), thomas.debeer@ugent.be (T. De Beer), Chris.Vervaet@UGent.be (C. Vervaet).

https://doi.org/10.1016/j.ijpharm.2019.118756
Received 4 August 2019; Received in revised form 29 September 2019; Accepted 30 September 2019
Available online 21 October 2019

mechanism of a highly water-soluble API from lipid microspheres composed of Compritol 888 and paraffin wax (Pivette et al., 2012). Vervaeck et al. demonstrated that long chain FAs, such as stearic acid (SA) and behenic acid (BA), are excellent matrix formers in a multi-particulate controlled release dosage form manufactured by prilling (Vervaeck et al., 2013). FAs are used as a versatile pharmaceutical excipient (e.g. binder during melt granulation (Maejima et al., 1997; Bhagwat et al., 2008), taste masking (Qi et al., 2006; Robson et al., 1999), (enteric) hot-melt coating (Patil et al., 2012; Kulah and Kaya, 2011; Jannin and Cuppok, 2013) or matrix for sustained drug release via melt agglomeration (Bhagwat et al., 2008; Voinovich et al., 2000).

As the API can be dissolved or suspended in a (mixture of) molten FA during processing, the physical state of the drug during prilling could affect processing as well as the characteristics of the prills. As Vervaeck et al. focused on API/FA solutions (e.g. metoprolol tartrate (MPT) in BA) (Vervaeck et al., 2015), no information is available on the feasibility of prilling API/FA suspensions, as indicated by Séquier *et al.* (Séquier et al., 2014). Therefore, the aim of current study was to evaluate the potential of prilling for APIs suspended in molten FA. To fully understand the effect of suspended API particles in the molten FA during processing, the API-FA solutions of Vervaeck et al. (i.e. MPT in BA) were further investigated in this study (Vervaeck et al., 2015; Vervaeck et al., 2013).

In the first part of this study, the processability of API/FA suspensions via prilling was evaluated. An API/FA suspension was defined as processable when prills could be generated without thermal degradation, nozzle obstruction or sedimentation during processing at a sufficiently high drug load. The second part of this study characterised the final prills in terms of size, shape, solid state and dissolution profile. Droplet formation at the nozzle and its solidification in liquid nitrogen was visualized via high-speed imaging and quantified via rapid heat-cool differential scanning calorimetry (RHC). Metformin hydrochloride (MET) and paracetamol (PAR) were selected as model APIs, both highly soluble in water and insoluble in FA. Formulations with varying drug load (10–40%) and FA chain lengths (C14–C22) were produced to evaluate the processability of API/FA suspensions and their prill characteristics.

2. Materials and methods

2.1. Materials

Four long chain saturated FAs with different carbon chain lengths (C14, C16, C18 and C22) were evaluated: myristic acid (MA) with a C14 purity of 99.2%, palmitic acid (PA) with a C16 purity of 99.3%, SA with a C18 purity of 98.3% (Mosselman, Ghlin, Belgium) and BA with a C22 purity of 88.9% (Radiacid 0560, Oleon, Ertvelde, Belgium). The melting point of MA, PA, SA and BA is 53 °C, 62 °C, 68 °C and 75 °C, respectively. These FAs were combined with MET (Granules, Hyderabad, India), PAR (Mallinckrodt, Manchester, UK) or MPT (Esteve Quimica, Barcelona, Spain) as model drugs with a water solubility of 297 g/l, 8 g/l and 682 g/l (20 °C), respectively. Prills were dissolved in absolute (> 99.8%) ethanol (VWR, Radnor, United States). Dissolution media were made with sodium lauryl sulfate (SLS) (Fagron, Waregem, Belgium), potassium dihydrogen phosphate (VWR, Radnor, United States), sodium hydroxide (Sigma Aldrich, Saint Louis, United States) and hydrochloric acid (VWR, Radnor, United States).

2.2. Methods

2.2.1. Prilling

Prills were manufactured using a modified Prilldrop® device (Peira, Turnhout, Belgium), depicted in Fig. 1. FAs were heated to 30 °C above their melting temperature and subsequently the API was added to the molten FA under continuous stirring (350 rpm – 8 cm long stirring bar). After 15 min of intensive stirring at a constant temperature, the prilling process was started by applying an initial pressure (1 bar) on the reservoir to feed the viscous API/FA suspension to the thermostated nozzle ($T_{nozzle} = T_{melt\ FA} + 30$ °C; inner nozzle diameter: 445 µm). The flow rate through this nozzle was controlled with a pneumatic valve system with a calibrated drop time for non-viscous pure water. Individual API/FA droplets were formed at the nozzle by lowering the pressure on the vessel (0.1 bar) and adjusting the valve opening (drop time: 0.03 s; interval: 0.10 s). Under these conditions, approximately 150 API/FA suspension droplets/min were formed at the nozzle. The individual droplets were quench cooled in liquid nitrogen whereby a solid matrix system (prill) was formed.

The effect of drug load (10–40%) and FA chain length (C14–C22) on the processability of API/FA suspensions and the characteristics of prills was evaluated, manufacturing 12 different formulations (Table 1). All formulations were produced in duplicate to evaluate the drug content, solid state, as well as size and shape of the prills for two independent batches, while the dissolution profile after manufacturing and during storage was evaluated for one batch.

2.2.2. Thermogravimetric analysis (TGA)

The thermal stability of pure FAs and APIs under extreme processing conditions (i.e. 2 h at 105 °C) was screened via TGA (Hi-res TGA 2950, TA instruments, Leatherhead, UK). The samples (± 15 mg) were heated to 110 °C and kept isothermal for 2 h while recording the weight loss.

2.2.3. Hot stage microscopy

The solubility of MET and PAR in molten FAs was determined via hot stage microscopy (Leica, Wetzlar, Germany). Therefore, a physical mixture of 1% API in FA was filled in a quartz crucible (diameter: 15 mm) and heated to 30 °C above the melting temperature of the FA. Physical mixtures were obtained after sieving (180 µm) all compounds followed by homogenous blending (Turbula mixer type T2F, W.A. Bachofen Maschinenfabrik, Basel, Switzerland). The API was defined as insoluble in the molten FA when API crystals were still visible (magnification: 100×) after maintaining the physical mixture at the maximum processing temperature ($T_{melt\ FA}$ + 30 °C) for 1 h.

2.2.4. Rapid heat-cool differential scanning calorimetry (RHC)

To evaluate the crystallization kinetics of API/FA solutions and suspensions, a prototype RHC (TA Instruments, Leatherhead, UK) equipped with a liquid nitrogen cooling unit was used. Tzero calibration was performed at 250 °C/min with sapphire disks, while an indium standard was used for the temperature and enthalpy calibration. 220 ± 20 µg of pure FA or physical mixtures (125 µm) were filled in low mass (≤ 2.1 mg) aluminium RHC crucibles. To obtain a pre-treatment similar to the prilling process, all samples were kept 30 °C above the melting temperature of the used FA for 10 min to ensure complete melting of FA and to allow sufficient time for MPT crystals to dissolve. Subsequently, the sample was rapidly cooled (250 °C/min) to a specific crystallization temperature (68.0 °C, 69.0 °C, 70.0 °C, 70.5 °C, 71.0 °C, 71.5 °C and 72.0 °C) and kept isothermal for 2 min. Thereafter the sample was cooled down (500 °C/min) to −50 °C and a new pre-treatment was started. The time needed to reach the FA crystallization peak maximum when the crystallization temperature was reached, was used to compare the crystallization rate of the samples.

2.2.5. Size and shape of the suspended APIs

Since API particles and/or agglomerates can obstruct the nozzle, particle size and shape distribution of the suspended APIs was determined. The particle size and shape of the dry API powder was analysed via a dynamic image analyser (Camsizer XT, Retsch Technology, Haan, Germany) equipped with an air pressure dispersion unit set at 180 – 185 kPa (X-jet, Retsch Technology, Haan, Germany). Powders were analysed in triplicate to calculate the mean Feret diameter and weighted average aspect ratio (ratio of the minimal to the maximal

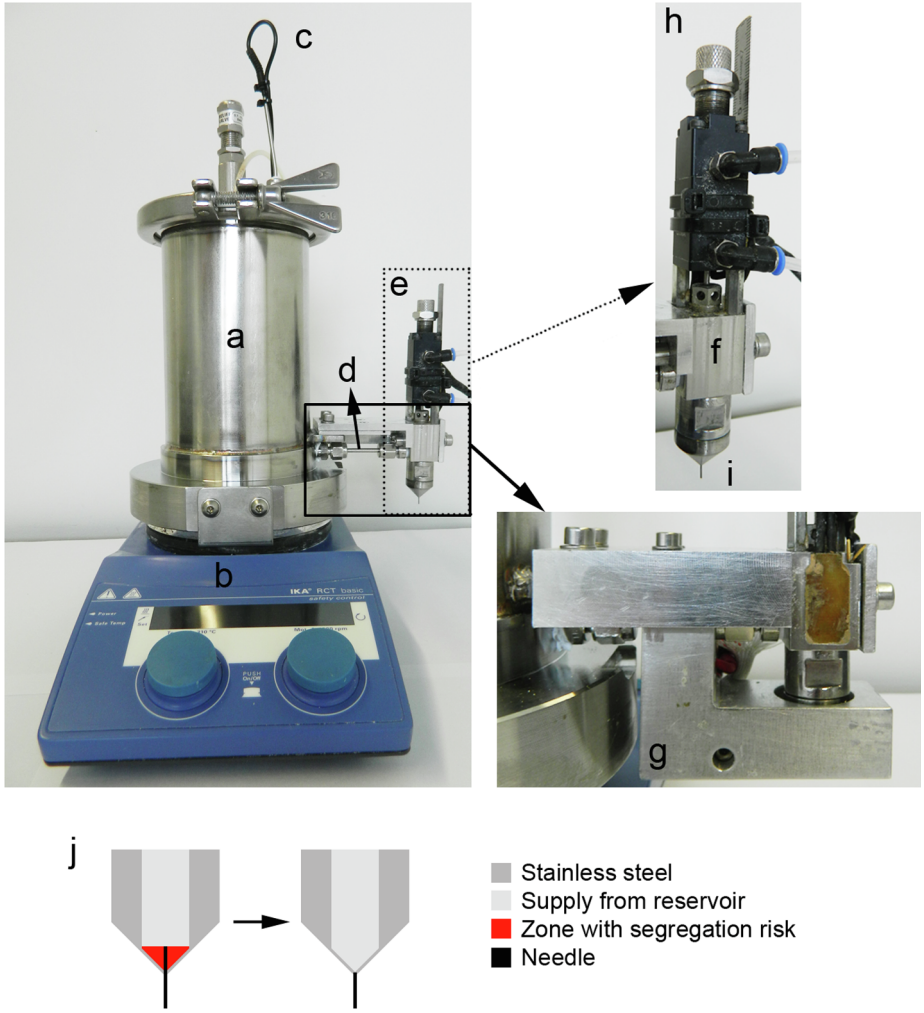

Fig. 1. Design of the modified Prilldrop device. (a) melt reservoir, (b) reservoir heater and magnetic stirrer, (c) temperature sensor with feedback loop, (d) connection tube between reservoir and nozzle, (e) thermostated nozzle, (f) original nozzle heater, (g) extra nozzle heater, (h) valve, (i) needle (internal diameter: 445 μm) (j) schematic overview of the final seamless nozzle.

Table 1
Overview of API/FA suspensions and the processing temperature used to evaluate the influence of drug load and type of FA on the processability. Average drug content of the two formulated batches and maximum relative drug content deviation of prills as a function of processing time at 6 min intervals over a 1 h period are displayed.

Processing temperature and drug content			
Formulation	Processing temp $T_{melt\ FA}$ + 30 °C	Average ± SD (%)	Max relative deviation (%)
10% MET in BA	105	10.09 ± 0.18	3.60
20% MET in BA	105	19.09 ± 1.05	−12.91
30% MET in MA	83	29.78 ± 0.59	− 4.81
30% MET in PA	92	30.14 ± 0.70	7.25
30% MET in SA	98	29.94 ± 0.58	4.21
30% MET in BA	105	29.28 ± 0.66	− 9.02
40% MET in BA	105	40.36 ± 0.80	3.76
10% PAR in BA	105	10.60 ± 0.33	12.69
20% PAR in MA	83	20.29 ± 0.52	5.45
20% PAR in PA	92	20.81 ± 0.41	7.72
20% PAR in SA	98	21.31 ± 0.54	11.92
20% PAR in BA	105	21.26 ± 0.99	12.59

Feret diameter) based on a volume distribution. Additionally, the shape of the dry API particles was visualized by scanning electron microscopy (SEM) (Quanta 200F, Thermo Fisher Scientific, Waltham, USA) after sputtering with a gold coating (thickness: 45–50 nm) using an Emtech SC7620 sputter coater (Quorum Technologies, Laughton, United Kingdom) to improve the electron conductivity of the samples.

To evaluate API agglomeration in a hydrophobic environment such as molten FAs, laser diffraction (Malvern Mastersizer S long bench, Malvern Instruments, Malvern, UK) was applied on dispersions of the API in Miglyol 812® (IOI Oleo, Hamburg, Germany). As a pre-treatment, dispersions were vortexed and subsequently sonicated for 10 min (i.e. standard method), ultrasonically vibrated (4 h – 40 kHz) or high shear mixed (10 min – 6000 rpm) in a Silverson L4R (East Longmeadow, United States). After transfer to the wet sample dispersion unit (1500 rpm) to obtain an obscuration of 10–30%, the samples were analysed using a 300RF lens (Malvern Instruments, Malvern, UK). d_{50} and d_{90} were determined on a volume-based distribution after performing measurements in triplicate.

2.2.6. Drug content

Homogeneity of drug content in the prills as a function of processing time was assessed over a 1 h period at 6 min intervals. Drug content was spectrophotometrically determined using a double beam spectrophotometer (UV-1650PC, Shimadzu, Antwerp, Belgium) after dissolving ± 35 mg prills (i.e. 5 prills) in absolute ethanol. MET concentrations were calculated based on a calibration curve ranging from 1.9 to 9.6 μg/ml at a wavelength of 239 nm. PAR concentrations were calculated based on a calibration curve ranging from 2.2 to 13.0 μg/ml at a

wavelength of 250 nm. The deviation in drug content relative to the targeted drug content for each time interval and the average drug content of the two independent batches of each formulation were calculated.

Via Raman microscopic mapping (Raman Rxn1 Microprobe, Kaiser Optical Systems, Ann Arbor, USA) the API distribution in the FA matrix was evaluated. Cross sections of prills were scanned in both the x and y directions with a 10× objective lens in area mapping mode using an exposure time of 5 s with 3 accumulations and a step size of 50 µm. Data collection and data transfer were automated using HoloGRAMS™ data collection software (version 2.3.5, Kaiser Optical Systems, Ann Arbor, USA), the HoloMAP™ data analysis software (version 2.3.5, Kaiser Optical Systems, Ann Arbor, USA) and Matlab software (version 7.1, The MathWorks, Natick, MA, USA). Each mapping was evaluated via multivariate curve resolution (MCR) to evaluate the homogeneity of the API distribution in the FA matrix. Therefore, all spectra of each mapping were merged in a data matrix and baseline corrected via Pearson's method and subsequently normalized.

2.2.7. High-speed imaging

Droplet formation at the nozzle and their solidification in liquid nitrogen was visualized using a Photron Mini AX200 high-speed camera (San Diego, USA) available at DyMaLab at Ghent University, together with adequate lighting. The camera was equipped with a fixed focus macro lens (Tamron, New York, USA), having a 90 mm focal length. Image resolution and frame rate were adjusted during the different experiments in order to optimize the visualization of droplet formation and solidification events. The ranges of the image resolutions used were 1024 × 725 to 640 × 464 pixels, and the ranges of the frame rates were 4000–6400 fps.

2.2.8. Size and shape of the prills

Surface and cross section of prills were examined by SEM (Quanta 200F, Thermo Fisher Scientific, Waltham, USA) after sputtering with a gold coating using an Emtech SC7620 sputter coater (Quorum Technologies, Laughton, United Kingdom) to improve the electron conductivity of the samples.

Size and shape (i.e. aspect ratio and sphericity) of the prills were evaluated via a dynamic imaging analysis technique (QICPIC, Sympatec, Clausthal-Zellerfeld, Germany). All batches were analysed in triplicate (± 2 g) and Windox 5 software (Sympatec, Clausthal-Zellerfeld, Germany) was used to calculate the mean Feret diameter, weighted average aspect ratio and sphericity (ratio of the perimeter of the equivalent circle, P_{EQPC}, to the real perimeter) based on a volume distribution. The average values of the two batches per formulation were reported.

2.2.9. Rheology of molten mixtures

The viscosity of pure FA, API/FA suspensions and API/FA solutions was measured using a stress controlled Haake™ Mars III rheometer (Thermo Fisher Scientific, Waltham, USA) with a 60 mm titanium parallel plate geometry. Depending on their viscosity, samples were analysed with flat, non-polished plates or serrated plates to obtain reliable rheological results that were not influenced by apparent wall slip or protrusion flow (Barnes, 1995; Marchesini et al., 2015). Via a Peltier temperature controller, the plates were kept at the standard processing temperature used for prilling (i.e. $T_{melt\ FA}$ + 30 °C).

The samples were measured using a gap between the plates of 2 ± 0.1 mm, this ensured that the gap was at least 10 times larger than the particle size of the suspended particles to obtain a continuous medium (Mendes et al., 2014). The shear rate was varied from 3000 to 0.1 s^{-1} or 500 to 0.01 s^{-1} in 15 steps (log scale) for measurements performed with flat or serrated plates, respectively. Each step was held for 30 s to give the sample enough time to stabilize and record an accurate torque value. Since sedimentation could occur during sample loading, the shear rate was varied from higher to lower values to obtain repeatable rheological results (Marchesini et al., 2015; Mueller et al., 2010). All measurements were performed in triplicate, and the average and standard deviation were calculated.

2.2.10. Solid state characterisation

The solid state of pure components, physical mixtures (180 µm) and corresponding prills was analysed via X-ray diffraction (XRD) and Raman spectroscopy. XRD patterns were recorded with a D5000 Cu Kα diffractor (λ = 0.154 nm) (Siemens, Karlsruhe, Germany) with a voltage of 40 mV in the angular range of $4^\circ < 2\theta < 60^\circ$ using a step scan mode with step size of 0.02° and counting time of 1 s/step.

Raman spectra were recorded in triplicate with a Raman Rxn1 spectrometer (Kaiser Optical Systems, Ann Arbor, USA) equipped with an air-cooled CCD detector and a 785 nm Invictus NIR diode laser over the 0–1800 cm^{-1} range with a resolution of 4 cm^{-1}, an exposure time of 5 s and 3 accumulations. Data collection and data transfer were automated using HoloGRAMS™ data collection software (version 2.3.5, Kaiser Optical Systems, Ann Arbor, USA). Spectra were corrected by standard normal variate (SNV) pre-processing and centred prior to data analysis using Simca 14.1.0 (Umetrics, Umeå, Sweden).

2.2.11. In vitro drug release

In vitro dissolution tests were performed using USP dissolution apparatus 2 (paddle speed: 100 rpm) in combination with sinker baskets to prevent floating of the hydrophobic prills. The dissolution apparatus consisted of a VK 7010 dissolution system coupled to a VK 8000 automatic sampling station (Vankel, New Jersey, USA). Prills equivalent with 150 mg API (sink conditions) were added to 900 ml dissolution medium maintained at 37 ± 0.5 °C. Four types of dissolution media were used to evaluate the influence of pH and/or surfactants on the drug release profile: demineralized water, phosphate buffer (pH 7.4), 0.1 M HCl (pH 1) and 0.1% SLS aqueous solution. In case of dissolution tests on MET prills, 5 ml samples were withdrawn on 10 time points over a 5 h, 8 h or 12 h period, depending on the drug release rate. For dissolution tests on PAR prills, ten 5 ml samples were withdrawn during 24 h (i.e. 0.5, 1, 2, 4, 6, 8, 12, 16, 20 and 24 h). Those samples were analysed spectrophotometrically using a double beam spectrophotometer (UV-1650PC, Shimadzu, Antwerp, Belgium) to calculate the API concentration from a calibration curve ranging from 1.5 to 14.7 µg/ml at a wavelength of 234 nm for MET samples and from 1.7 to 16.9 µg/ml at 243 nm for PAR samples.

Similarity between the dissolution profiles obtained in different media was evaluated by calculating the similarity factor f_2 as described by Shah et al. (Eq. (1)), where R_t and S_t represent the cumulative drug release at sample point t of the sample in the reference medium and the sample in the alternative medium, and with n equal to the number of total sample points. As described by Shah et al., maximum one sample point with a cumulative drug release higher than 85% may be included to avoid bias in the similarity assessment. Therefore, depending on the drug release profile, 5–10 sample time points were taken into account to calculate the similarity factor. Dissolution profiles are considered similar if f_2 is ≥ 50, which corresponds to an average difference of less than 10% at all sampling time points (Shah et al., 1998).

$$f_2 = 50\log_{10}\left\{\left[1 + \frac{1}{n}\sum_{t=1}^{n}(S_t - R_t)^2\right]^{-1/2} * 100\right\} \quad (1)$$

2.2.12. Storage

Processing and storage of API/FA formulations can change the crystalline state of formulation components and/or induce interactions at molecular level between the different components (Becker et al., 2015; Vervaeck et al., 2014; Del Gaudio et al., 2009; Garti and Sato, 1988). Therefore, a stability study was performed whereby immediately after production the prills were packed in hermetically sealed bags under controlled circumstances (< 35% RH) and stored at 25 °C and

40 °C for 1 week, 1 month, 3 months and 6 months. Beside evaluation of the solid state after storage, the drug release profile was re-evaluated throughout the stability study in demineralized water and 0.1% SLS solution for MET and PAR prills, respectively, by evaluation of the similarity factor.

2.2.13. X-ray tomography

The specific surface area and porosity of prills before and after dissolution were evaluated using high-resolution X-ray computed tomography. The scans were performed at the custom-designed micro-CT setup HECTOR of the Ghent University Centre for X-ray Tomography (UGCT) (Masschaele et al., 2013). The tube voltage was set to 90 kV and the power of the system was 10 W. The exposure time for each project image was 1000 ms and 2401 projection images were recorded over a 360° rotation. The raw data was reconstructed using Octopus Reconstruction (TESCAN-XRE, Ghent, Belgium), using the Paganin phase retrieval algorithm (Paganin et al., 2002). An isotropic voxel size of 4 μm was used to analyse at least 15 prills for one batch per formulation.

Bespoke data processing was developed in Avizo Fire 9.5 (FEI Visualization Sciences Group, Burlington, United States) to determine the specific surface area of each prill from the 3D X-ray tomography data. Initially, the tomography images were denoised using an anisotropic diffusion filter in order to improve the robustness of the subsequent steps. Thresholding was used to determine a binary volume from the denoised data. A marker-based Watershed algorithm was applied on the binary volume to separate the prills and facilitate the analysis of individual prills. The number of prills analysed is slightly smaller (i.e. at least 10 prills per formulation) than the total number of prills imaged as only prills visible in their entirety and clearly separated from each other were analysed. The specific surface area was determined per prill and used to normalize surface area to the prill volume. The porosity was determined from the binary volume of all prills.

3. Results and discussion

3.1. Processability

MET and PAR were selected as model APIs to evaluate the processability of API/FA suspensions since thermogravimetric analyses indicated no thermal degradation of these APIs or FAs under extreme processing conditions (i.e. 2 h at 105 °C), while hot stage microscopy demonstrated their insolubility in molten FA under the applied processing conditions (Fig. S1).

Prilling of API/FA suspensions initially resulted in obstruction of the 445 μm nozzle due to solidification of FA and/or (agglomeration of) the suspended particles. Solidification of molten FA in the nozzle was avoided by installing an extra heating pad around the nozzle of the prilling equipment (Fig. 1g). However, nozzle obstruction still occurred as API/FA suspensions were used instead of solutions. As the nozzle diameter was limited (i.e. 445 μm), only a few large API particles (d_{90}) and/or agglomerates of the hydrophilic API in the molten hydrophobic FA could cause nozzle obstruction. The particle size distribution of the API in the molten FA was estimated via laser diffraction analysis where the API was dispersed in a liquid phase with a hydrophobicity similar to FAs (Table 2). While MET particles remained almost intact ($d_{90\ wet} \approx d_{90\ dry}$) when dispersed in the liquid phase, PAR agglomerates were broken up ($d_{90\ wet} \ll d_{90\ dry}$). Unfortunately, nozzle obstruction occurred and the particle size (d_{90}) could not be sufficiently reduced by the addition of a surfactant (0.2% polysorbate 80 or 0.2% sorbitan monolaurate in migylol® 812), ultrasonic vibration or high shear mixing. For example, d_{90} of unsieved PAR remain intact (76 ± 3 μm), only a slight decrease to 66 μm was observed in case a high shear mixer was used. However, sieving of the API (using a 50 and 150 μm sieve for MET and PAR, respectively) prior to their addition to the molten FA was efficient to reduce $d_{90\ wet}$ (≤ 60 μm) of the suspended particles and consequently prevent obstruction of the nozzle (445 μm) during processing (Table 2), indicating the importance of size of the API particle suspended in the FA phase.

Table 2
Particle size (d_{50}, d_{90} and span) and shape (aspect ratio) of both model APIs measured under dry and wet conditions, before and after sieving: MET – 50 μm sieve, PAR – 150 μm sieve.

API powder: size and shape									
Measuring conditions		MET				PAR			
		d_{50} (μm)	d_{90}	Span	AR	d_{50} (μm)	d_{90}	Span	AR
Dry	Unsieved	111	277	2.26	0.73	25	505	20.69	0.71
	Sieved	17	37	1.84	0.81	13	38	2.59	0.77
Wet	Unsieved	118	220	1.83	NA	42	76	1.41	NA
	Sieved	33	60	1.76	NA	23	52	2.23	NA

The design of the prilling device was also essential towards the quality of the prills. Whereas previous studies processed homogeneous API/FA solutions, this study focused on API/FA suspensions, which are intrinsically susceptible to sedimentation (Vervaeck et al., 2013; Nutan et al., 2010). Hence, it was essential to identify the critical parts of the equipment with a high probability of API sedimentation (e.g. due to inadequate flow or stirring) and to subsequently modify the process to ensure a constant drug content in the prills throughout the manufacturing process. While the flow inside the narrowed and shortened connection tube between reservoir and nozzle (Fig. 1d) and inside the seamless nozzle (Fig. 1j) was sufficient to avoid sedimentation of the suspended API, it was observed that the mixing intensity inside the reservoir remained the most critical parameter towards API sedimentation. In case a smaller stirring bar was used, sedimentation occurred at the seams of the melt reservoir and the drug content of the prills increased in function of processing time. For example, prilling a 30% MET in BA formulation with a smaller stirring bar resulted in a linearly increasing drug content from 25.5 to 28.8% during a 1 h production process. Using of a stirring bar with a diameter equal to the diameter of the melt reservoir avoided API sedimentation in the melt reservoir and yielded prills with a stable drug content and a maximum relative drug content deviation below 15% for all time points per formulation, in accordance with the European Pharmacopoeia guidelines (Table 1).

Initial screening experiments revealed that sieved (150 μm) PAR in BA suspensions were processable up to a drug load of 20%, while sieved (50 μm) MET in BA suspensions were processable up to a drug load of 40%. Since viscosity is a critical process parameter during droplet formation at the nozzle, this difference in maximum processable drug load could be attributed to the higher viscosity of PAR in BA suspensions in comparison with MET in BA suspensions at equal drug loads as illustrated in Fig. 2 (Séquier et al., 2014; Vervaeck et al., 2014; Rawle, 2010; Mastropietro et al., 2013). Rheological experiments also revealed an almost Newtonian behaviour for MET suspensions, while distinct shear thinning was observed for PAR suspensions.

Since the measuring temperature was kept consistently 30 °C above the melting temperature of the selected FA, varying the FA chain length of the formulations did not significantly change the viscosity (Fig. S2). Consequently, the observed differences in viscosity of MET and PAR formulations can be attributed to the varying size and shape of MET and PAR suspended particles. Sieved MET (50 μm) and PAR (150 μm) had a mean Feret diameter of 17 μm (span 1.84) and 13 μm (span 2.59), respectively (Table 2). Due to the lower particle size of PAR in comparison with MET, the number of particles and consequently the number of particle-particle interactions at equal drug load was higher in the PAR suspensions, resulting in a higher viscosity. Additionally, the degree of

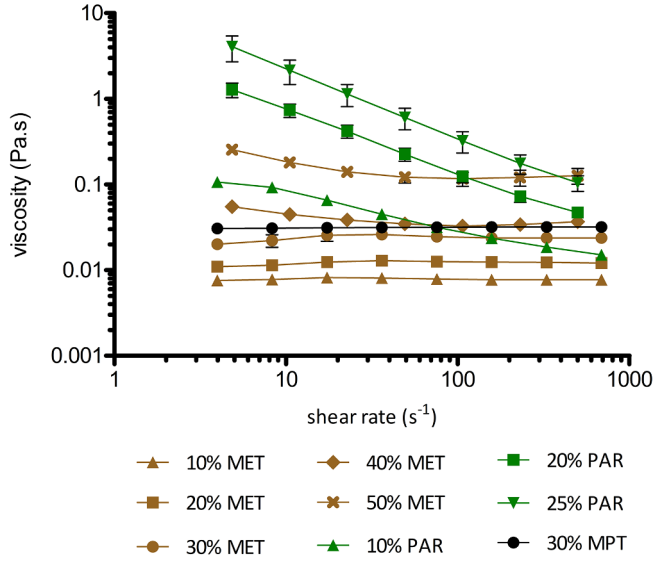

Fig. 2. Viscosity of API/BA suspensions and a 30% MPT in BA solution at processing temperature ($T_{melt\ FA}$ + 30 °C) in function of shear rate.

particle-particle interactions in PAR suspensions was favoured by the rod shape of PAR particles (AR: 0.765) in comparison with the more spherical MET particles (AR: 0.810) as demonstrated by SEM (Fig. 3). The elongated PAR particles were more resistant to flow as a result of their larger specific surface area and non-suitable particle orientation. As these particle-particle interactions are weak, their effect was more pronounced at low shear rates what explained the shear thinning behaviour of the PAR formulations (Genovese, 2012; Mastropietro et al., 2013; Mueller et al., 2010; Rawle, 2010).

Based on the initial screening experiments, the flow curve obtained for a 20% PAR in BA suspension defined the maximum viscosity of a formulation at a specific shear rate that allowed processing via prilling. This observation was in accordance with the measured viscosity of successfully processed MET (10–40%) in BA and 30% MPT in BA formulations. As a remark, Del Gaudio et al. estimated the characteristic viscosity at the nozzle via the Cross model (Robson et al., 1999; Patil et al., 2012). In the current study, multiple processes such as stirring, pumping and droplet formation at the nozzle were ongoing during the prilling process and influenced the processability. Consequently, a specific shear rate could not be defined and beyond the scope of this article (Séquier et al., 2014). The current viscosity limit was selected based on formulations with an observed processability.

In conclusion, the processability of API/FA suspensions was dominated by the size and shape of the API powder and independent of the FA chain length. A lower API particle size and aspect ratio resulted in more particle-particle interactions and a higher viscosity at equal drug load.

3.2. Size and shape of the prills

SEM imaging revealed a characteristic structure of the MET and PAR prills, i.e. prills had an orifice at their surface that was connected to a cavity inside the prill (Fig. 4a and b). This phenomenon was independent of drug load, which is in contrast with MPT/FA solutions tested by Vervaeck et al. (2013). While MPT in BA prills with a low drug load (i.e. 10% and 20%) had an orifice and cavity similar to the MET and PAR suspension prills, at 30% MPT in BA the prills were completely solid and spherical despite an expulsion on their surface (Fig. 4c). To explain the observed differences in the shape of prills produced from a suspension versus a solution, MPT in BA formulations as described by Vervaeck et al. were further investigated in this study (Vervaeck et al., 2015; Vervaeck et al., 2013; Vervaeck, 2015). High-speed imaging of the droplet formation at the nozzle of a 30% MPT in BA formulation and a 10% MET in BA formulation revealed that the droplets became immediately spherical when released from the nozzle. The time needed for the droplets to become spherical was < 11.6 ms for the 30% MPT in BA and < 22.8 ms for the 10% MET in BA (Fig. 5) formulation, respectively. This spherical shape was maintained during their falling motion before reaching the liquid nitrogen bath.

Consequently, the differences in prill shape originated from droplet solidification in liquid nitrogen. Via high-speed imaging and RHC experiments, it was demonstrated that the differences in shape can be attributed to a difference in FA crystallization rate between API/FA suspensions and API/FA solutions with a high drug load.

Via RHC experiments, the FA crystallization rate was evaluated for multiple formulations. To simulate the first part of the prilling process, physical mixtures were pretreated 30 °C above the melting temperature of the corresponding FA, before they were rapidly cooled down (250 °C/min) and kept isothermal just below the melting point of the used FA. The time needed to reach the BA crystallization peak maximum during isothermal crystallization was short and comparable for all API/BA suspensions, independent of API type or drug load (Fig. 6). High-speed camera imaging indicated that the solidification of an API/FA suspension droplet (Fig. S3) was initiated at a specific point (i.e. the point of origin) on the surface of the droplet and continued from here in all directions. An outer shell was quickly formed over most of the droplet and solidification of the liquid core (i.e. crystal growth) moved inwards from this outer layer. Due to the shrinking behaviour of FA

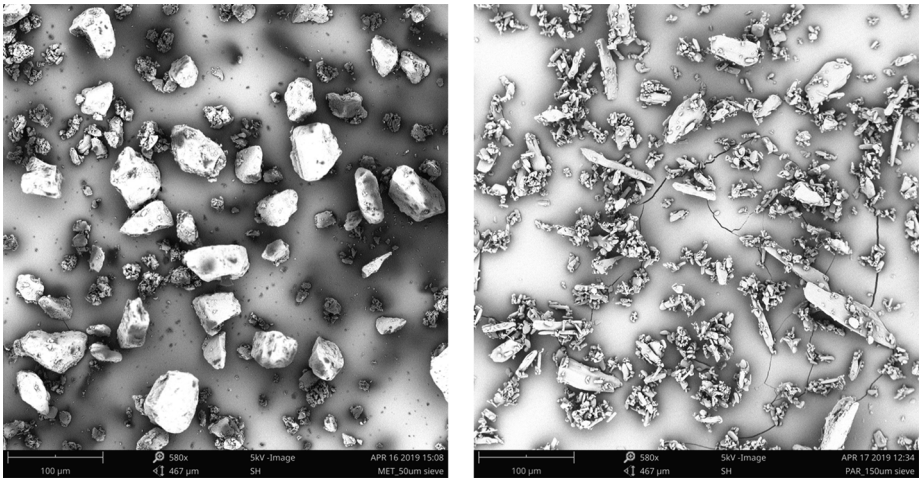

Fig. 3. SEM-images: sieved (left) MET (50 µm) and (right) PAR (150 µm) powder particles.

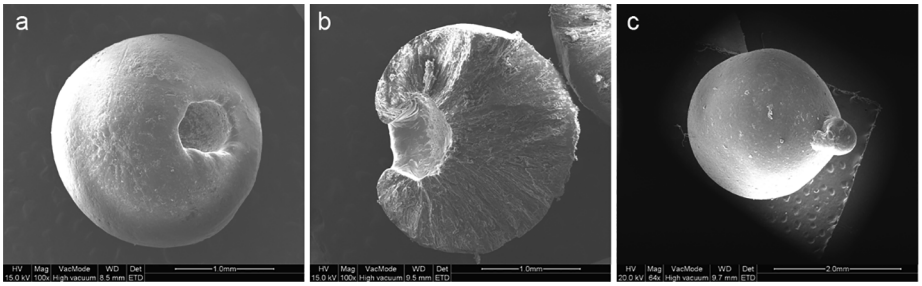

Fig. 4. SEM-images: surface (a, c) and cross-section (b) of prills containing (a, b) 20% MET in BA and (c) 30% MPT in BA.

during solidification, a cavity was formed inside the prill which was connected to an orifice at the surface of the prill, in accordance to the shrinking unsolidified core model of Séquier et al. (2014). Wu et al. (2007), Brockmann et al. (2000). The orifice was formed at the location where the outer shell crystallised the latest (i.e. opposite to the point of origin). Another hypothesis to explain the formation of the cavity inside the prills was that part of the liquid core was expelled when the surface of the droplet shrank upon solidification. However, this hypothesis was

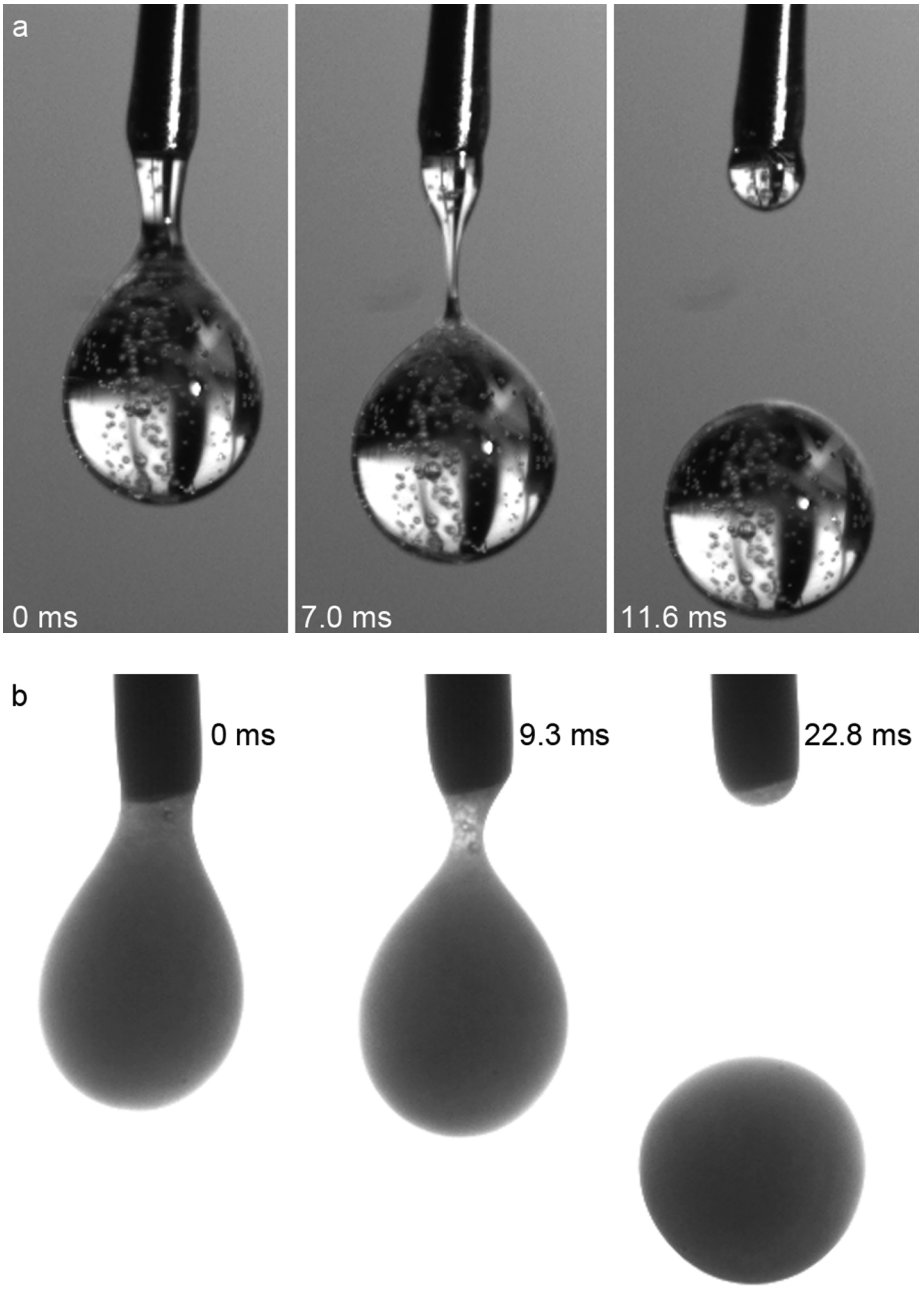

Fig. 5. Spherical droplet formation at the nozzle of (a) a transparent 30% MPT in BA solution, (b) an opaque 10% MET in BA suspension in function of time.

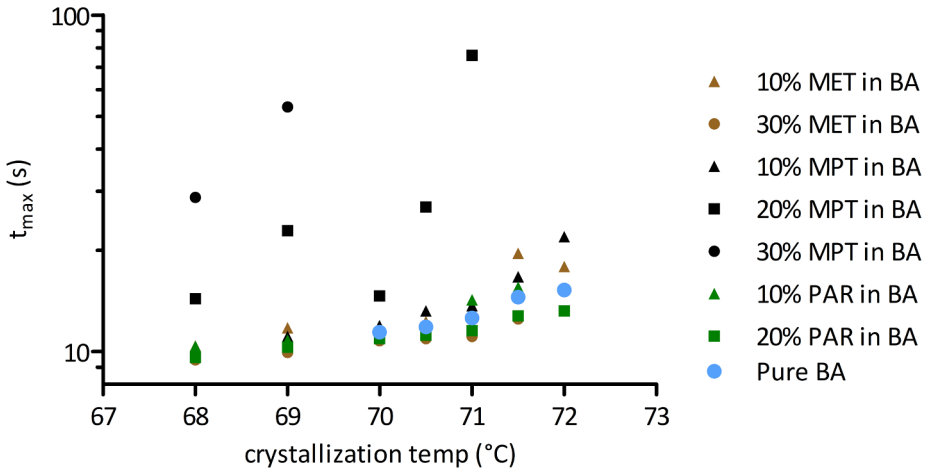

Fig. 6. Time needed to reach the BA crystallization peak maximum during isothermal crystallization in RHC as a measure for the droplet solidification rate. Both API/BA suspensions and solutions with varying drug loads were analysed at different crystallization temperatures.

rejected since no core expulsion was observed via high-speed imaging. Hence, although a cavity was formed during solidification, no mass loss did occur.

In contrast, RHC experiments indicated that more time was needed to reach the BA crystallization peak maximum for MPT/BA solutions with a higher MPT load (Fig. 6). Since a 20% MPT in BA formulation still resulted in prills with a cavity, it was assumed that once a threshold crystallization rate was reached (i.e. between 20% and 30% MPT in BA) droplet solidification was no longer dominated by the shrinking properties of FAs. Visualisation of droplet solidification of a 30% MPT in BA solution via high-speed imaging showed the creation of an expulsion at the surface of the prills (Fig. 7). When the surface of this droplet slowly solidified from the point of origin, the unsolidified core of the droplet due to the inner pressure created by the liquid core in a solid outer shell. The expulsion was formed at the location where the outer shell crystallised the latest.

When analysing the final size and shape of API/FA suspension-based prills (Table 3), no trends in function of drug load or FA chain length were detected. MET and PAR prills had a mean Feret diameter of 2.30 mm (span 0.10) and 2.42 mm (span 0.08), an average aspect ratio of 0.905 ± 0.007 and 0.917 ± 0.012, and a sphericity of 0.937 ± 0.004 and 0.921 ± 0.007, respectively. Hence, these spherical prills had excellent flow properties.

3.3. Solid state characterisation

XRD patterns demonstrated that the crystallinity of MET, PAR and FAs did not change by thermal processing via prilling and during storage. Characteristic peaks of MET for 2θ (e.g. 12.2° and 17.7°) and PAR (e.g. 23.5° and 26.5°) showed up in the physical mixture and prills even after 6 months of storage while no additional peaks were observed, confirming that MET and PAR remained in their original crystalline form (Fig. S4). Stability of the FA crystallinity was in agreement with the observation of Kobayashi, who stated that molten FAs exclusively crystallized into the thermodynamically stable C-form (Kobayashi, 1988; Singleton et al., 1950). The absence of specific interactions between the components and the preservation of crystallinity during 6 months storage was confirmed via Raman spectroscopy: no changes in the characteristic Raman bands of MET, PAR and FAs were observed (Fig. S5).

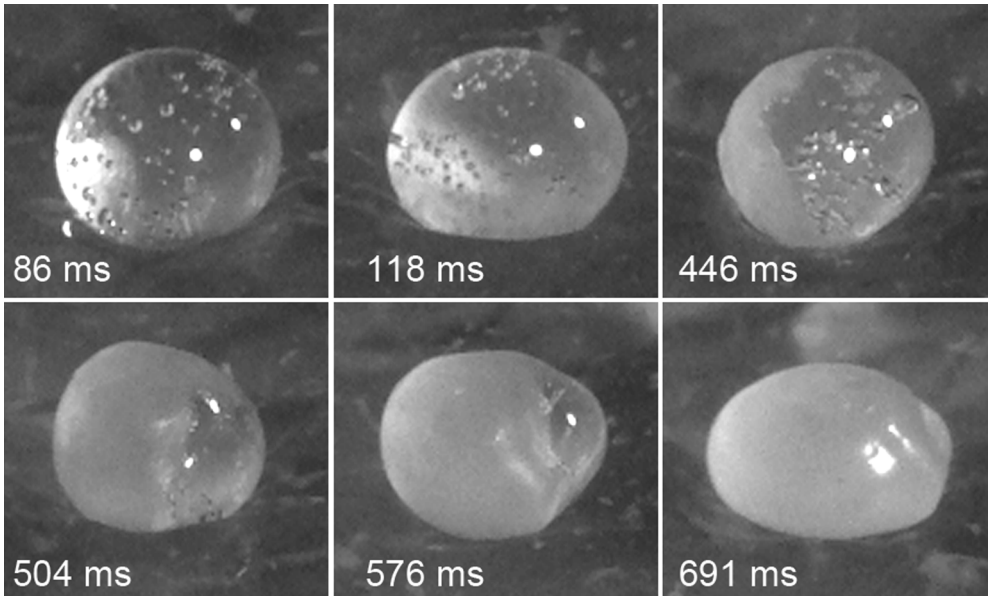

Fig. 7. Formation of an expulsion at the surface of a 30% MPT in BA prill during fast solidification in liquid nitrogen. Time after the droplet made first contact with liquid nitrogen is indicated on the images.

Table 3
Overview of average particle size and shape of MET and PAR prills. No trends in function of drug load and/or FA chain length could be observed.

MET prills				
	BA prills: influence of drug load			
	10	20	30	40
d_{50} ± SD (mm)	2.35 ± 0.02	2.31 ± 0.07	2.28 ± 0.05	2.21 ± 0.07
span	0.10	0.08	0.08	0.10
sphericity	0.93	0.93	0.94	0.94
aspect ratio	0.91	0.90	0.91	0.91
	30% MET prills: influence of FA type			
	MA	PA	SA	BA
d_{50} ± SD (mm)	2.31 ± 0.02	2.32 ± 0.01	2.33 ± 0.04	2.28 ± 0.05
span	0.12	0.10	0.10	0.08
sphericity	0.94	0.94	0.94	0.94
aspect ratio	0.90	0.90	0.91	0.91

PAR prills				
	BA prills: influence of drug load			
	10[a]	20		
d_{50} ± SD (mm)	2.47	2.38 ± 0.06		
span	0.07	0.09		
sphericity	0.92	0.93		
aspect ratio	0.93	0.93		
	20% PAR prills: influence of FA type			
	MA	PA	SA	BA
d_{50} ± SD (mm)	2.44 ± 0.02	2.44 ± 0.02	2.40 ± 0.07	2.38 ± 0.06
span	0.09	0.09	0.09	0.09
sphericity	0.92	0.92	0.91	0.93
aspect ratio	0.91	0.91	0.91	0.93

[a] Only 1 batch could be analysed.

3.4. In vitro drug release

A higher drug load of a hydrophilic API can create an extensive channel network in a hydrophobic matrix by dissolution of the API in the dissolution medium, resulting in a faster drug release rate (Pivette et al., 2012; Rosiaux et al., 2014). This mechanism was observed for all MET and PAR in BA prills (Figs. 8b and 9b), except for the 10% MET in BA prills. Despite the lower drug load in the BA prills with 10% MET and consequently low potential to form a channel network in the matrix, 63% of the drug load was released in 1 h, compared to 37%, 32% and 49% release from BA prills containing 20%, 30% and 40% MET, respectively. This deviating dissolution profile was attributed to an inhomogeneous API distribution, as demonstrated via X-ray tomography and Raman mapping. X-ray tomography showed that MET crystals (white regions in Fig. 10a) were preferentially located at the border of prills containing 10% MET, while at higher drug content the drug was homogeneously distributed throughout the prill. The inhomogeneous distribution of 10% MET in the BA matrix was confirmed by monitoring the intensity of a characteristic MET peak (737 cm^{-1}) relative to a characteristic BA peak (1295 cm^{-1}) via Raman mapping (Fig. 10c): the relative intensity of the MET signal decreased from the surface to the centre of a 10% MET in BA prill. These variations in relative intensity were not observed at higher drug loads, as illustrated for a 30% MET in BA prill in Fig. 10d. This inhomogeneous API distribution can be linked to the low viscosity of the 10% MET in BA molten mixture (Fig. 2), allowing a higher mobility of MET particles before solidification of the prills in comparison with MET formulations with a higher drug load and PAR formulations. It should also be noted that complete drug release was not obtained for 10% MET in BA prills, as some MET crystals remained isolated in the BA matrix in comparison with the higher MET drug loaded prills.

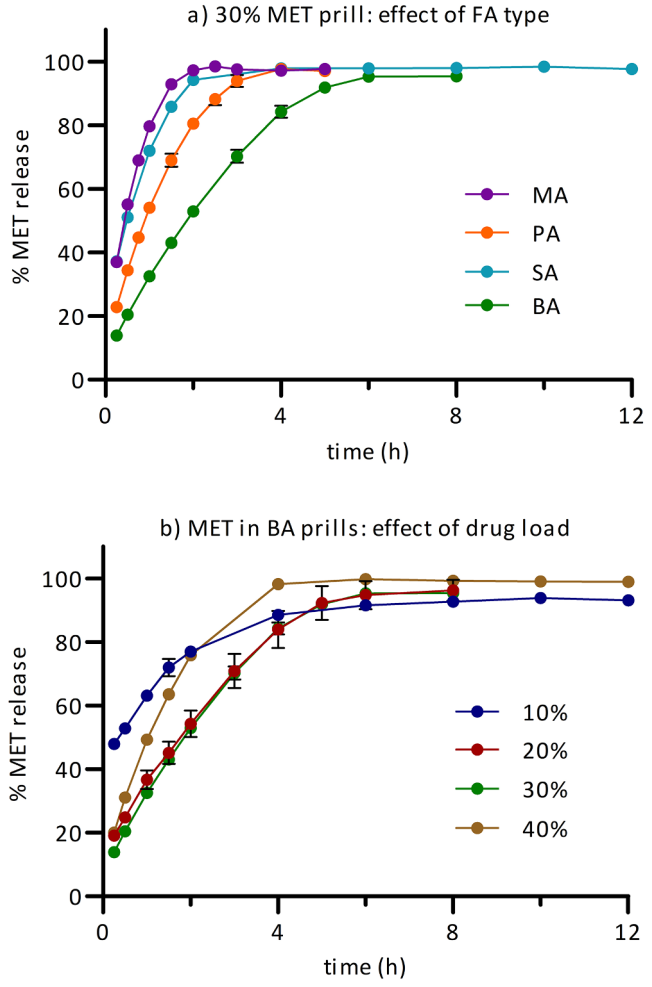

Fig. 8. Mean dissolution profile (± SD) of MET prills in demineralized water in function of (a) FA chain length and (b) drug load.

Similar to Vervaeck et al. (2013); Figs. 8a and 9a illustrate a faster drug release rate when the FA chain length decreased, except for SA-based prills. The faster release from the SA matrix was linked to the higher porosity of these formulations independent of the API as identified via X-ray tomography (Fig. 10b and Table 4). Since the time needed to reach the FA crystallization peak maximum during isothermal crystallization of the FA was comparable (10.1 ± 0.7 s) and fast for all 30% MET formulations (independent of the FA grade), the origin of multiple pores in the SA-based formulations could not be linked to its behaviour during cooling and is therefore still under research.

As illustrated in Fig. 8, complete drug release of MET in demineralized water depended on the drug load and FA chain length, varying between 2.5 and 6 h. In contrast, drug release from PAR prills (Fig. 9a) was slower: even after 24 h drug release was not complete when demineralized water was used as dissolution medium. This observation was correlated with the lower water solubility of PAR in comparison with MET (Rosiaux et al., 2014).

mps@123456 As seen in Fig. 9b, the addition of 0.1% SLS or a phosphate buffer to the dissolution medium enhanced the drug release of 20% PAR from BA prills. As demonstrated by Vervaeck et al., the effect of the phosphate buffer was the result of (partial) ionization of the carboxylic acid group of FA, which increased the matrix hydrophilicity

Table 4
Average specific surface area, its relative standard deviation and the porosity of at least 10 MET prills per formulation based on X-ray tomography image analysis.

X-ray tomography data processing			
Formulation	Specific surface area[a]		Porosity
	Average (mm^{-1})	Relative standard deviation (%)	(%)
10% MET in BA	3.30	8.85	0.17
20% MET in BA	3.25	4.25	0.11
30% MET in MA	3.40	2.72	0.24
30% MET in PA	3.27	4.53	0.06
30% MET in SA	3.89	3.54	0.48
30% MET in BA	3.06	3.60	0.04
40% MET in BA	3.94	6.13	0.43
10% PAR in BA	4.34	14.54	0.75
20% PAR in MA	5.17	9.1	1.23
20% PAR in PA	3.89	7.42	0.36
20% PAR in SA	7.78	10.57	2.41
20% PAR in BA	4.07	5.92	0.24

[a] Normalized surface area to prill volume.

(Vervaeck et al., 2013). Since this (partial) ionization was not achieved at pH 1 (0.1 M HCl), the release profile was similar (f_2 = 85) with the profile obtained in demineralized water (pH 5.4). Although the SLS concentration was below the critical micellar concentration, the surfactant improved the wettability of the prills and as a result the release rate of PAR in the dissolution medium (Pivette et al., 2012). In a phosphate buffer or 0.1% SLS solution as dissolution medium drug release from short chain FA prills was complete within 12 h and 16 h (Fig. 9c). No significant effect of the dissolution medium on the release rate of MET formulations was observed during preliminary experiments, due to the high water solubility.

No significant differences (f_2 > 50) in drug release profile were observed after storing MET and PAR prills during 6 months at 25 °C and 40 °C. This is in accordance with the solid state analysis that did not reveal transformations.

Although all prills had a similar size with a constant drug content per mass unit and the drug release profiles were reproducible, variations in the size of the cavity inside the prills could disturb volumetric capsule filling with a correct API dose. Therefore, the variation in size of the cavity within each formulation was evaluated via specific surface area based on X-ray tomography scanning images (Table 4). For all MET formulations, independent of drug load or FA chain length, the relative standard deviation of the specific surface area was less than 10%. SEM images revealed that PAR prills have a rougher microscopic surface (Fig. 11), which was also reflected by the large specific surface area of PAR prills compared to MET prills. Therefore, the correlation between the specific surface area and the size of the cavity inside the prill was disturbed.

Moreover, a high specific surface area was related to a high porosity of the prills, as it captured the entire surface including cracks and pores. Both specific surface area and porosity of the prills affected the drug release rate, where a low specific surface area/porosity slowed down the dissolution process. The slowest drug release was observed for the BA formulations (Figs. 8a and 9a for MET and PAR formulations, respectively) with the smallest porosity per formulation.

As a conclusion, the presence of a cavity inside the prill is not problematic since the drug release profiles were reproducible and high-speed imaging analysis in combination with RHC measurements demonstrated that the cavity was formed due to shrinking during cooling without mass loss.

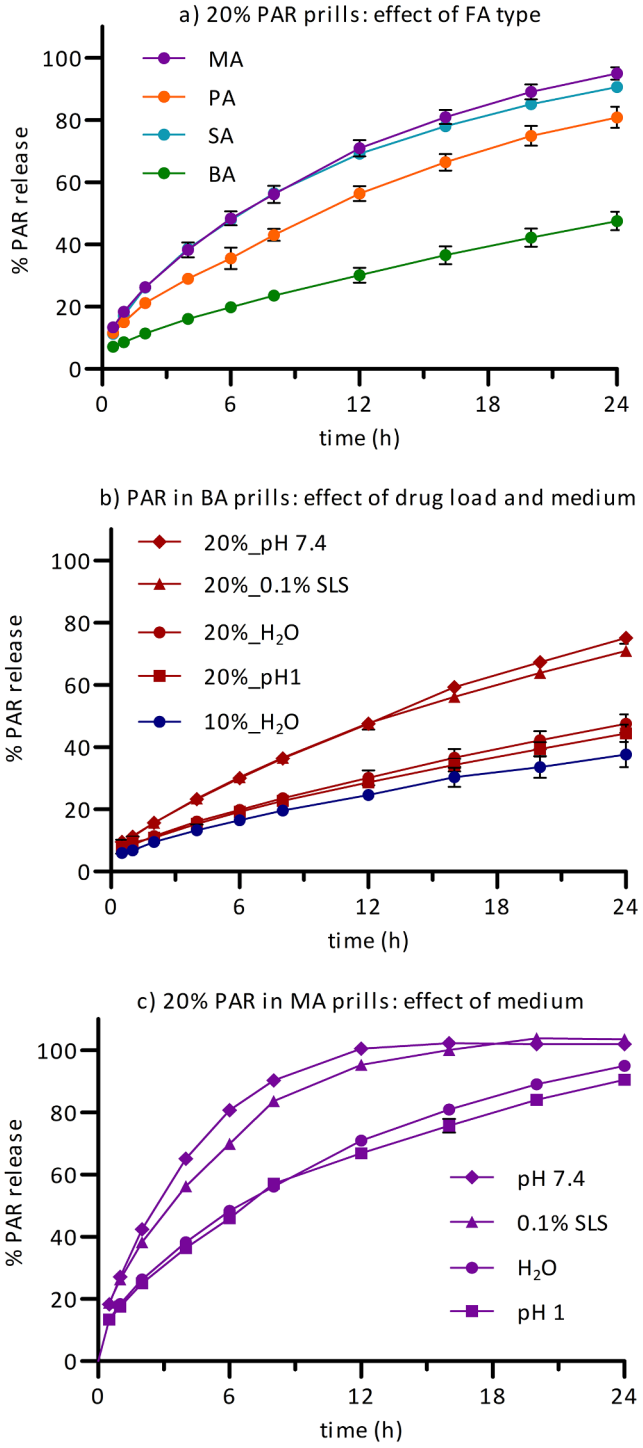

Fig. 9. Mean dissolution profile (± SD) of PAR prills in function of (a) FA chain length in demineralized water, (b) drug load and (b, c) dissolution medium.

4. Conclusion

This study indicated that prilling of API/FA suspensions is a promising technique for the production of lipid-based multi-particulate

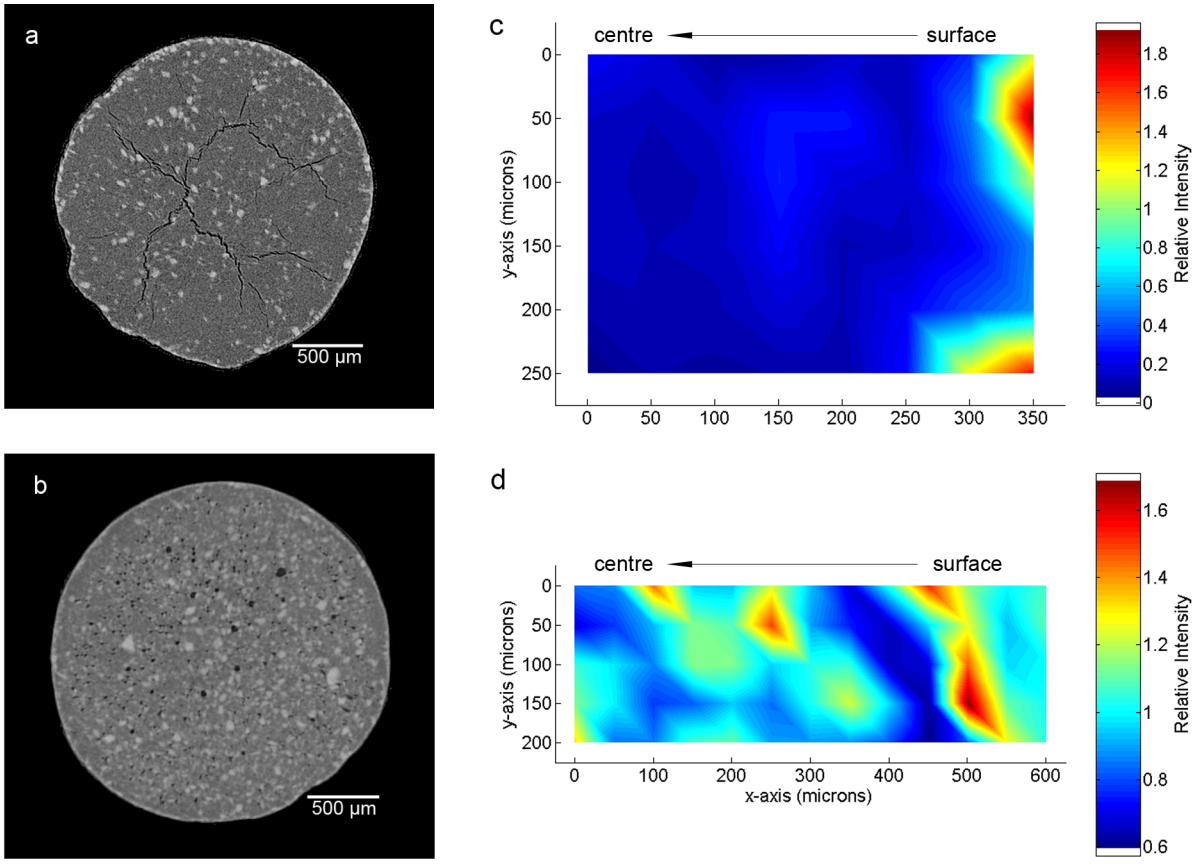

Fig. 10. Visualisation of the inhomogeneous MET distribution in 10% MET in BA prill (a, c) in comparison with 30% MET in SA (b) and BA (d) prills. X-ray tomography cross section of a) 10% MET in BA prills with an inhomogeneous MET distribution, b) 30% MET in SA prills with a high porosity. As a remark, a grayscale was chosen for optimal visibility. (c, d) Raman mapping on a cross-section of a prill reveals the inhomogeneous MET distribution in 10% MET in BA prills (c) in comparison with the distribution in 30% MET in BA prills (d). A red colour corresponds to a high relative intensity (high MET content), while a blue colour corresponds to a low relative intensity (low MET content). (For interpretation of the references to colour in this figure legend, the reader is referred to the web version of this article.)

spherical dosage forms. The processability of API/FA suspensions was only limited by the viscosity of the molten mixture, which was mainly affected by the size and shape of the API particles, but was independent of the FA chain length. API/FA suspensions showed a fast re-crystallization of their FA fraction upon cooling, resulting in prills with an orifice at their surface that was connected to a cavity inside the prill, without negatively influencing the reproducibility of the drug release. The collected API/FA suspension-based prills were spherical with a smooth surface and had a particle size independent of the drug load and/or FA chain length. In vitro drug release evaluation revealed a faster drug release at higher drug load, higher API water solubility and shorter FA chain length. In future experiments upscaling of the prilling process will be studied to increase the production capacity. A system where droplets will be formed by the laminar jet break-up of a continuous flow via a vibrating nozzle will be evaluated. Subsequently, the droplets will be solidified during their falling motion in a cooling tower.

Declaration of Competing Interest

The authors declare that they have no known competing financial

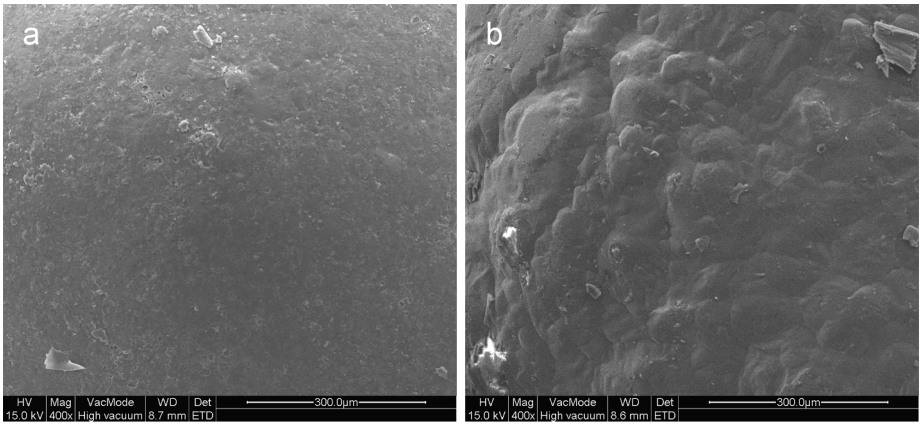

Fig. 11. SEM images of (a) smooth 30% MET in BA prill surface and (b) rough 10% PAR in BA prill surface.

interests or personal relationships that could have appeared to influence the work reported in this paper.

Acknowledgements

E. De Coninck acknowledges the Special Research Fund of Ghent University for a PhD scholarship.

Appendix A. Supplementary material

Supplementary data to this article can be found online at https://doi.org/10.1016/j.ijpharm.2019.118756.

References

Aleksovski, A., Van Bockstal, P.J., Roskar, R., Sovany, T., Regdon Jr., G., De Beer, T., et al., 2016. Comparison of metoprolol tartrate multiple-unit lipid matrix systems produced by different technologies. Eur. J. Pharm. Sci. 88, 233–245.

Aleksovski, A., Vervaet, C., Dreu, R., 2016. Hot-melt extrusion and prilling as contemporary and promising techniques in the solvent free production of solid oral dosage forms, based on solid dispersions. Macedonian Pharm. Bull. 62, 3–24.

Barnes, H.A., 1995. A review of the slip (wall depletion) of polymer solutions, emulsions and particle suspensions in viscometers: its cause, character, and cure. J. Non-Newton Fluid. 56 (3), 221–251.

Becker, K., Salar-Behzadi, S., Zimmer, A., 2015. Solvent-free melting techniques for the preparation of lipid-based solid oral formulations. Pharm. Res. 32 (5), 1519–1545.

Bhagwat, D.D., Kawtikwar, P., Sakarkar, M.D., 2008. Sustained release matrices of verapamil HCl using glyceryl monosterate and stearic acid. Res. J. Pharm. Tech. 1, 405–409.

Brockmann, R., Demmering, G., Kreutzer, U., Lindemann, M., Plachenka, J., Steinberner, U., 2000. Fatty Acids. Ullmann's encyclopedia of industrial chemistry. 40, 6th ed. Wiley-VCH Verlag GmbH & Co, Weinheim, Germany, pp. 73–116.

Del Gaudio, P., Russo, P., Rosaria Lauro, M., Colombo, P., Aquino, R.P., 2009. Encapsulation of ketoprofen and ketoprofen lysinate by prilling for controlled drug release. AAPS PharmSciTech 10 (4), 1178–1185.

Garti, N., Sato, K., 1988. Crystallization and Polymorphism of Fats and Fatty Acids. Marcel Dekker, Inc., New York.

Genovese, D.B., 2012. Shear rheology of hard-sphere, dispersed, and aggregated suspensions, and filler-matrix composites. Adv. Colloid Interface Sci. 171, 1–16.

Jannin, V., Cuppok, Y., 2013. Hot-melt coating with lipid excipients. Int. J. Pharm. 457 (2), 480–487.

Jannin, V., Musakhanian, J., Marchaud, D., 2008. Approaches for the development of solid and semi-solid lipid-based formulations. Adv. Drug Deliv. Rev. 60 (6), 734–746.

Kobayashi, M., 1988. Vibrational spectroscopic aspects of polymorphism and phase transition of fats and fatty acids. In: In: Garti, N., Sato, K. (Eds.), Crystallization and polymorphism of fats and fatty acids 31. Marcel Dekker, Inc., New York, pp. 139–187.

Kulah, G., Kaya, O., 2011. Investigation and scale-up of hot-melt coating of pharmaceuticals in fluidized beds. Powder Technol. 208 (1), 175–184.

Maejima, T., Osawa, T., Nakajima, K., Kobayashi, M., 1997. Preparation of spherical beads without any use of solvents by a novel tumbling melt granulation (TMG) method. Chem. Pharm. Bull. (Tokyo). 45 (3), 518–524.

Marchesini, F., Naccache, M., Abdu, A., Alicke, A., Mendes, P.R.D., 2015. Rheological characterization of yield-stress materials: Flow pattern and apparent wall slip. Appl. Rheol. 25, 32–41.

Martins, R.M., Siqueira, S., Machado, M.O., Freitas, L.A., 2013. The effect of homogenization method on the properties of carbamazepine microparticles prepared by spray congealing. J. Microencapsul. 30 (7), 692–700.

Masschaele, B., Dierick, M., Van Loo, D., Boone, M.N., Brabant, L., Pauwels, E., et al., 2013. HECTOR: a 240kV micro-CT setup optimized for research. In: Xu, H., Wu, Z., Tai, R. (Eds.), 11th International Conference on X-Ray Microscopy. Iop Publishing Ltd, Bristol.

Mastropietro, D.J., Nimroozi, R., Omidian, H., 2013. Rheology in pharmaceutical formulations - a perspective. J. Dev. Drugs 02, 6.

Mehrez, A., Ookawara, S., Ali, A.H.H., Suzuki, M., 2014. A numerical study on cooling-solidification process of urea particles in prilling tower. J. Chem. Eng. Jpn. 47 (8), 628–634.

Mendes, P.R.D., Alicke, A.A., Thompson, R.L., 2014. Parallel-plate geometry correction for transient rheometric experiments. Appl. Rheol. 24 (5), 1–10.

Mueller, S., Llewellin, E.W., Mader, H.M., 2010. The rheology of suspensions of solid particles. Proc. Royal Soc. A 466 (2116), 1201–1228.

Nutan, M.T.H., Reddy, I.K., 2010. General principles of suspensions. In: Kulshreshtha, A.K., Singh, O.N., Wall, G.M. (Eds.), Pharmaceutical suspensions. Springer, pp. 39–65.

Paganin, D., Mayo, S.C., Gureyev, T.E., Miller, P.R., Wilkins, S.W., 2002. Simultaneous phase and amplitude extraction from a single defocused image of a homogeneous object. J. Microsc. 206, 33–40.

Passerini, N., Qi, S., Albertini, B., Grassi, M., Rodriguez, L., Craig, D.Q., 2010. Solid lipid microparticles produced by spray congealing: influence of the atomizer on microparticle characteristics and mathematical modeling of the drug release. J. Pharm. Sci. 99 (2), 916–931.

Patil, A.T., Khobragade, D.S., Chafle, S.A., Ujjainkar, A.P., Umathe, S.N., Lakhotia, C.L., 2012. Development and evaluation of a hot-melt coating technique for enteric coating. Braz. J. Pharm. Sci. 48 (1), 69–77.

Pivette, P., Faivre, V., Mancini, L., Gueutin, C., Daste, G., Ollivon, M., et al., 2012. Controlled release of a highly hydrophilic API from lipid microspheres obtained by prilling: analysis of drug and water diffusion processes with X-ray-based methods. J. Control. Release 158 (3), 393–402.

Qi, S., Deutsch, D., Craig, D.Q., 2006. An investigation into the interaction between taste masking fatty acid microspheres and alkaline buffer using thermal and spectroscopic analysis. J. Pharm. Sci. 95 (5), 1022–1028.

N. Rahamnian, M. Homayoonfard, (Eds.), 2012. A comparison of co-current and counter-current modes of operation in urea prilling tower. In: International conference on process engineering and advanced materials. Kuala Lumpur, Malaysia.

Rahmanian, N., Homayoonfard, M., Alamdari, A., 2013. Simulation of urea prilling process: an industrial case study. Chem. Eng. Commun. 200 (6), 764–782.

Rahmanian, N., Naderi, S., Supuk, E., Abbas, R., Hassanpour, A., 2015. Urea finishing process: prilling versus granulation. Procedia Eng. 102, 174–181.

Rawle, A.F., 2010. Analytical tools for suspension characterization. In: Kulshreshtha, A.K., Singh, O.N., Wall, G.M. (Eds.), Pharmaceutical suspensions: from formulation development to manufacturing. Springer New York, New York, Ny, pp. 177–230.

Reitz, C., Kleinebudde, P., 2007. Solid lipid extrusion of sustained release dosage forms. Eur. J. Pharm. Biopharm. 67 (2), 440–448.

Robson, H.J., Craig, D.Q., Deutsch, D., 1999. An investigation into the release of cefuroxime axetil from taste-masked stearic acid microspheres. Part 1: the influence of the dissolution medium on the drug release profile and the physical integrity of the microspheres. Int. J. Pharm. 190 (2), 183–192.

Rosiaux, Y., Jannin, V., Hughes, S., Marchaud, D., 2014. Solid lipid excipients - matrix agents for sustained drug delivery. J. Control. Release 188, 18–30.

Séquier, F., Faivre, V., Daste, G., Renouard, M., Lesieur, S., 2014. Critical parameters involved in producing microspheres by prilling of molten lipids: from theoretical prediction of particle size to practice. Eur. J. Pharm. Biopharm. 87 (3), 530–540.

Shah, V.P., Tsong, Y., Sathe, P., Liu, J.P., 1998. In vitro dissolution profile comparison-statistics and analysis of the similarity factor, f2. Pharm. Res. 15 (6), 889–896.

Singleton, W.S., Ward, T.L., Dollear, F.G., 1950. Physical properties of fatty acids. I. Some dilatometric and thermal properties of stearic acid in two polymorphic forms. J. Am. Oil Chem. Soc. 27 (4), 143–146.

Vervaeck, A., 2015. Prilling of fatty acids as innovative technology for oral controlled release multiple-unit systems. Ghent University, Ghent, Belgium.

Vervaeck, A., Saerens, L., De Geest, B.G., De Beer, T., Carleer, R., Adriaensens, P., et al., 2013. Prilling of fatty acids as a continuous process for the development of controlled release multiparticulate dosage forms. Eur. J. Pharm. Biopharm. 85, 587–596.

Vervaeck, A., Monteyne, T., Saerens, L., De Beer, T., Remon, J.P., Vervaet, C., 2014. Prilling as manufacturing technique for multiparticulate lipid/PEG fixed-dose combinations. Eur. J. Pharm. Biopharm. 88 (2), 472–482.

Vervaeck, A., Monteyne, T., Siepmann, F., Boone, M.N., Van Hoorebeke, L., De Beer, T., et al., 2015. Fatty acids for controlled release applications: a comparison between prilling and solid lipid extrusion as manufacturing techniques. Eur. J. Pharm. Biopharm. 97, 173–184.

Voinovich, D., Moneghini, M., Perissutti, B., Filipovic-Grcic, J., Grabnar, I., 2000. Preparation in high-shear mixer of sustained-release pellets by melt pelletisation. Int. J. Pharm. 203 (1–2), 235–244.

Wu, Y., Bao, C., Zhou, Y., 2007. An innovated tower-fluidized bed prilling process. Chin. J. Chem. Eng. 15 (3), 424–428.